Rotordynamic Analysis for Stepped-Labyrinth Gas Seals Using Moody's Friction-Factor Model

Tae Woong Ha*

Associate professor, Mechanical Engineering Department, Kyungwon University, Kyunggi-do 461-701, Korea

The governing equations are derived for the analysis of a stepped labyrinth gas seal generally used in high performance compressors, gas turbines, and steam turbines. The bulk-flow is assumed for a single cavity control volume set up in a stepped labyrinth cavity and the flow is assumed to be completely turbulent in the circumferential direction. The Moody's wall-friction -factor model is used for the calculation of wall shear stresses in the single cavity control volume. For the reaction force developed by the stepped labyrinth gas seal, linearized zeroth -order and first-order perturbation equations are developed for small motion about a centered position. Integration of the resultant first-order pressure distribution along and around the seal defines the rotordynamic coefficients of the stepped labyrinth gas seal. The resulting leakage and rotordynamic characteristics of the stepped labyrinth gas seal are presented and compared with Scharrer's theoretical analysis using Blasius' wall-friction-factor model. The present analysis shows a good qualitative agreement of leakage characteristics with Scharrer's analysis, but underpredicts by about 20 %. For the rotordynamic coefficients, the present analysis generally yields smaller predictied values compared with Scharrer's analysis.

Key Words : Stepped-Labyrinth Gas Seal, Rotordynamic Coefficients, Leakage, Moody's Wall-Friction Factor, Perturbation Method

Nomenclature

A : Circumferential cross-sectional area of control volume(m^2)
B : Height of labyrinth tooth(m)
C, c : Direct and cross-coupled damping coefficients(N · s/m)
C_r : Nominal clearance of seal(m)
D : Diameter of pipe(m)
d : Step height(m)
e : Absolute surface roughness(m)
f : Frequency ratio(Ω/ω)
f_B, f_M : Fanning friction factors defined by Blasius' and Moody's model
Fx, Fy : Components of seal reaction force in x-y coordinate system(N)
H : Local seal clearance(m)
K, k : Direct and cross-coupled stiffness coefficients(N/m)
L : Pitch of labyrinth tooth(m)
$\dot{m}$: Mass flowrate per circumferential length (kg/(s · m))
m, n : Coefficients for Blasius's friction model
P : Pressure(bar)
R : Gas constant(N · m/kg · K)
R_s : Inlet radius of seal rotor(m)
t : Time(s)
T : Temperature(K)
t_p : Labyrinth tooth width(m)
V : Average circumferential velocity in a labyrinth cavity(m/s)
Z_c : Compressibility factor
x, $\dot{x}$: Displacement and velocity of x-direction in rectangular coordinate(m, m/s)
y, $\dot{y}$: Displacement and velocity of y-direc-

* **E-mail** : Twha@mail.kyungwon.ac.kr
TEL : +82-31-750-5308; **FAX** : +82-31-750-5273
Associate professor, Mechanical Engineering Department, Kyungwon University Kyunggi-do, 461-701, Korea. (Manuscript **Received** August 28, 2001; **Revised** June 13, 2001)

tion in rectangular coordinate(m, m/s)
ε : Eccentricity ratio
θ : Angular coordinate
ρ : Fluid density (kg/m^3)
τ : Shear stress(N/m^2)
ν : Kinematic viscosity(m^2/s)
ω : Rotor angular velocity (rad/s)

Subscripts

0, 1 : Zeroth and first-order perturbations
s, r : Stator, rotor
i : i-th cavity

1. Introduction

Labyrinth seals are noncontact type seals that are commonly used in turbomachinery to reduce the leakage loss. In some cases, the fluid forces generated in the labyrinth seals cause severe rotordynamic instabilities. Therefore, the design engineer needs information about the dynamic characteristics of the labyrinth seals given by the stiffness, damping and inertia terms.

As shown in Fig. 1, see-through labyrinth seals are widely used in both compressors and turbines. Generally, teeth-on-stator seals are used for compressors and teeth-on-rotor seals are used for turbines. If the rotor steps up or down depending on the flowpath requirements, a divergent-stepped labyrinth or a convergent-stepped labyrinth seal configuration is used, respectively. These types of the seals have been used extensively in buffer seals, eye seals, and for seals on the back side of the impellers.

Since Alford(1965) proposed analytical models for the prediction of labyrinth seal forces, many theoretical and experimental analyses for the see-through labyrinth seals have been developed (Iwatsubo(1980), Jenny et al. (1984), Childs et al. (1986), Scharrer(1987), Ha et al. (1998)). However, for the stepped labyrinth seal there have been very few analytical works and no experimental work reported to date that provide quantitative description of the rotordynamic characteristics. Scharrer(1988) presented an analysis of the stepped labyrinth seal which was only a modification of the see-through labyrinth seal analysis using the Blasius' friction factor model for the shear stress definition(Childs et al. (1986)).

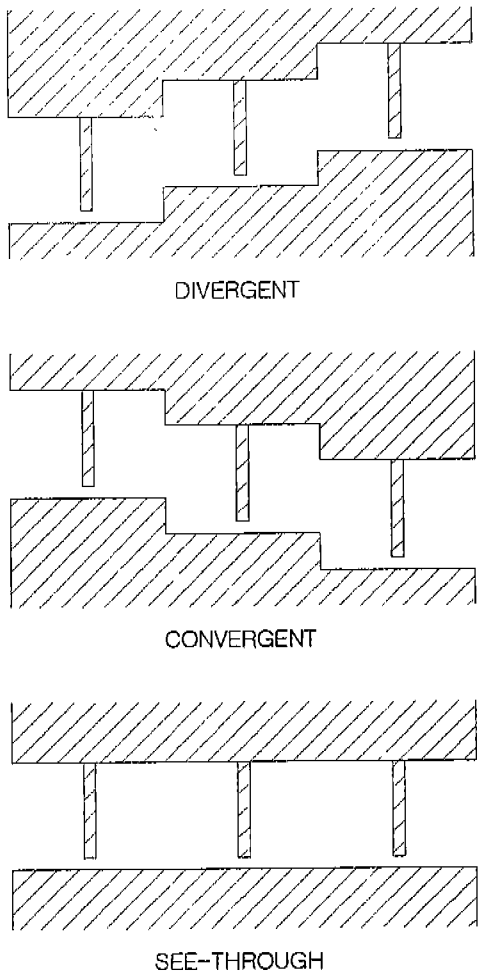

Fig. 1 Configurations of labyrinth seals

Most of the recent theoretical developments are based on a bulk flow theory that considers the shear stresses only at the fluid-wall interface but not within the fluid. Therefore, proper modeling of the wall friction is important for improving the accuracy of the prediction and facilitating the usage. As shown in Eqs. (1) and (2) respectively, Moody's wall friction factor model and Blasius' wall friction factor model can be utilized in the seal analysis.

$$f_M = 1.37\times10^{-3}\left[1+\left(20000\times\frac{e}{D}+\frac{10^6}{Rey}\right)^{\frac{1}{3}}\right] \quad (1)$$

$$f_B = n(Rey)^m \quad (2)$$

The Blasius' model, in which the friction factor is assumed to be a function of the Reynolds number(Rey) only, has been frequently used because of its simplicity. However, the Blasius' model can accurately reflect the change in the friction factor for small changes in a limited range of the Reynolds number(less than 1×10^5) as shown in Fig. 2, and has no functional dependence on relative roughness($\frac{e}{D}$). Nevertheless, the relative roughness does change in circumferential direction when the rotor whirls about its centered position. Therefore, the Moody' s model, which approximates Moody's diagram and assumes the friction factor to be a function of both the Reynolds number and relative roughness, conld be a better choice for the wall friction factor modeling purpose.

In the present work, leakage prediction and rotordynamic analysis of the teeth-on-stator stepped labyrinth seal with smooth rotor is developed using the Moody's wall friction factor model which is effective for a wide range of the Reynolds number and also incorporates the relative roughness effect. Validation of the present analysis is provided by comparing the results with the results of Scharrer(1988)'s analysis using the Blasius friction factor model.

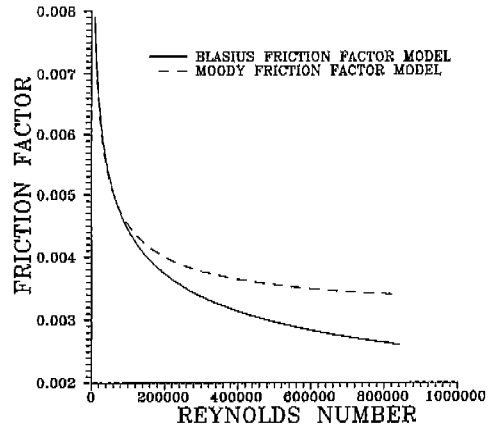

Fig. 2 Friction factor comparison for a smooth surface between the Blasius' and the Moody's model(empirical coefficients of Blasius model are n=0.07 and m=-0.25, e/D of Moody's model is 0. 0001)

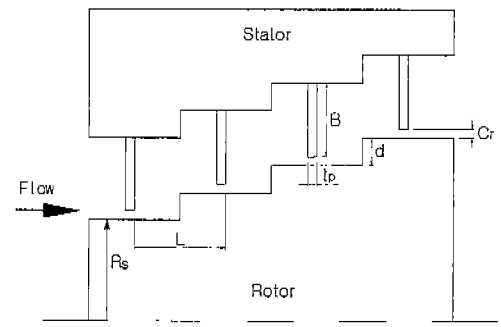

Fig. 3 A typical teeth-on-stator stepped labyrinth seal geometry

2. Mathematical Modeling

Figures 3 and 4 show a typical teeth-on-stator stepped labyrinth seal geometry and a control volume for theoretical analysis, respectively. Fluid flow in the stepped labyrinth seal cavity is developed by pressure difference between the entrance and exit of the seal and rotation of the rotor as in the case of the see-through labyrinth seal. However, a flow passage in the stepped labyrinth seal is so complicated that through-flow part and vortex-flow part can not be clearly divided. One control volume in each stepped labyrinth cavity is set up in the present analysis shown in Fig. 4.

The continuity equation for the control volume per unit circumferential length is given in Eq. (3), where A_i denotes i-th circumferential cross sectional area of the control volume and defined as $L_i\times(B_i+C_{ri}+B_{i+1}+C_{ri+1})/2$.

$$\frac{\partial}{\partial t}(\rho_i A_i)+\frac{1}{R_{si}}\frac{\partial}{\partial\theta}(\rho_i A_i V_i) + \frac{R_{si+1}}{R_{si}}\dot{m}_{i+1}-\dot{m}_i=0 \quad (3)$$

The circumferential momentum equation, Eq. (4), is derived from the equilibrium condition of related forces on the control volume in Fig. 5 where $a_{ri}=1$ and $a_{si}=(2\ B_i+L_i+d)/(L_i+d)$.

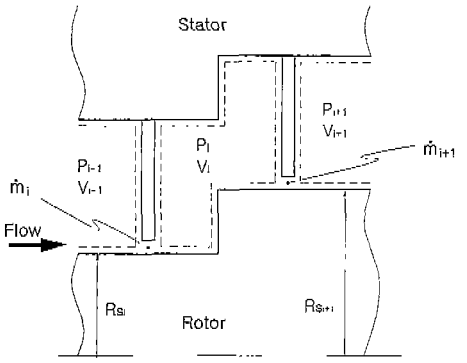

Fig. 4 Control volume for stepped labyrinth seal analysis

$$\rho_i A_i \frac{\partial}{\partial t}(V_i)+\frac{\rho_i V_i A_i}{R_{si}}\frac{\partial V_i}{\partial \theta}+\dot{m}_i(V_i-V_{i-1}) = -\frac{A_i}{R_{si}}\frac{\partial P_i}{\partial \theta}+\tau_{ri}a_{ri}(L_i+d) -\tau_{si}a_{si}(L_i+d) \quad (4)$$

τ_{si} and τ_{ri} for smooth stator and rotor surfaces can be defined using the Moody's wall friction factor model, Ha et al. (1996), as shown in Eqs. (5) and (6)

$$\tau_{si}=\frac{1}{2}\rho_i V_i^2 \left(1.37\times10^{-3}\left[1+\left(20000\times\frac{e}{Dh_i}+10^6\times\frac{\nu}{Dh_i V_i}\right)^{\frac{1}{3}}\right]\right) \quad (5)$$

$$\tau_{ri}=\frac{1}{2}\rho_i(R_{si}\omega-V_i)^2 \left(1.37\times10^{-3}\left[1+\left(20000\times\frac{e}{Dh_i}+10^6\times\frac{\nu}{Dh_i|R_{si}\omega-V_i|}\right)^{\frac{1}{3}}\right]\right) \quad (6)$$

where Dhi is a hydraulic diameter and defined by Eq. (7). The working fluid is assumed to be an ideal gas and the ideal gas law is used to eliminate the density terms.

$$Dh_i=\frac{2L_i(B_i+C_{ri})}{B_i+C_{ri}+L_i+d} \quad (7)$$

The mass flow rate per unit circumferential length($\dot{m}_i$) is defined by Eq. (8) which is Neumann(1964)'s experimental equation, where kinetic energy carryover factor(μ_{2i})(Vermes, 1961) and flow coefficient(μ_{1i})(Gurevitch, 1966) are shown in Eq. (9). In the present analysis, μ_{2i} is 1 since the step height(d) is much greater than the seal clearance(Cr)(Vermes, 1961).

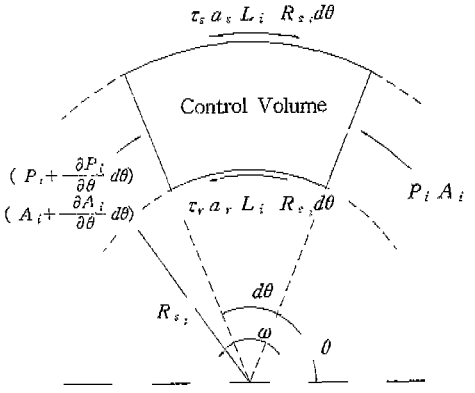

Fig. 5 Forces on control volume

$$\dot{m}_i=\mu_{1i}\mu_{2i}H_i\sqrt{\frac{P_{i-1}^2-P_i^2}{RT}} \quad (8)$$

$$\mu_{1i}=\frac{\pi}{\pi+2-5s_i+2s_i^2},\ s_i=\left(\frac{P_{i-1}}{P_i}\right)^{\frac{\gamma-1}{\gamma}}-1 \quad (9)$$

Assuming small whirling motion of the rotor about its geometric center, pressure, circumferential velocity, a local clearance can be expanded in terms of zeroth-order and first-order perturbation variables(Eq. (10)). Substitution of these perturbed variables into the governing equations yields a set of zeroth-order equations (Eqs. (11)~(12)) and first-order equations(Eqs. (13)~(14)) where the coefficients of G_i and Z_i are listed in the Appendix.

$$P_i=P_{0i}+\varepsilon P_{1i},\ H_i=C_r+\varepsilon H_{1i},\ V_i=V_{0i}+\varepsilon V_{1i} \quad (10)$$

Zeroth order equations

$$\frac{R_{si+1}}{R_{si}}\dot{m}_{i+1}-\dot{m}_i=0 \quad (11)$$

$$\dot{m}_i(V_{0i}-V_{0i-1})=\tau_{r0i}a_{ri}(L_i+d)-\tau_{s0i}a_{si}(L_i+d) \quad (12)$$

First order equations

$$G_{1i}\frac{\partial P_{1i}}{\partial t}+G_{2i}\frac{\partial P_{1i}}{\partial \theta}+G_{3i}\frac{\partial V_{1i}}{\partial \theta}+G_{4i}P_{1i} +G_{5i}P_{1i-1}+G_{6i}P_{1i+1} =-G_{7i}H_{1i}-G_{8i}\frac{\partial H_{1i}}{\partial t}-G_{9i}\frac{\partial H_{1i}}{\partial \theta} \quad (13)$$

$$Z_{1i}\frac{\partial V_{1i}}{\partial t}+Z_{2i}\frac{\partial V_{1i}}{\partial \theta}+Z_{3i}\frac{\partial P_{1i}}{\partial \theta}+Z_{4i}V_{1i}+Z_{5i}V_{1i-1} +Z_{6i}P_{1i}+Z_{7i}P_{1i-1}=Z_{8i}H_{1i} \quad (14)$$

3. Solution Procedure

The zeroth-order equations(Eqs. (11)~(12)) and leakage equation(Eq. (8)) define the leakage flowrate, the pressure distribution through cavities, and the circumferential flow velocity at each cavity when the rotor is located at its geometric center. Eq. (8) and Eq. (11) can be solved by using a numerical iteration method with the seal's entrance and exit condition specified to yield the leakage flowrate and the pressure distribution. Eq. (12) can also be solved by using a numerical root finding method to yield the cavity circumferential velocity. For choked flow, Fliegner's model(John(1979)), as given in Eq. (15), is used for the last seal strip.

$$\dot{m}=\frac{0.510\mu_{2i}}{\sqrt{RT}}PH \tag{15}$$

The first order equations(Eqs. (13)~(14)) define the pressure and velocity fluctuations resulting from the seal clearance change due to the rotor's whirling. With the assumption of an elliptical whirling orbit, Eqs. (13) and (14) can be reduced to linear algebraic equations and solved by using various numerical methods to yield the pressure perturbations. The x and y components of resultant forces of the stepped labyrinth seal can be calculated by integrating the pressure perturbations around and along the seal as follows :

$$F_x=-R_s\varepsilon\sum_{i=1}^{NC}\int_0^{2\pi}P_{1i}L_i\cos\theta d\theta \tag{16}$$

$$F_y=-R_s\varepsilon\sum_{i=1}^{NC}\int_0^{2\pi}P_{1i}L_i\sin\theta d\theta \tag{17}$$

where NC denotes the number of cavities. The rotordynamic coefficients for the stepped labyrinth gas seal can be defined by the following linearized force-displacement model(Eq. (18)). Finally, the rotordynamic coefficients of K, k, C, and c are determined from the relations between Eqs. (16)~(17) and Eq. (18).

$$-\begin{Bmatrix}F_x\\F_y\end{Bmatrix}=\begin{bmatrix}K & k\\-k & K\end{bmatrix}\begin{Bmatrix}x\\y\end{Bmatrix}+\begin{bmatrix}C & c\\-c & C\end{bmatrix}\begin{bmatrix}\dot{x}\\\dot{y}\end{bmatrix} \tag{18}$$

4. Results

This section presents the prediction of leakage and rotordynamic coefficients for the stepped labyrinth gas seal by using the Moody's wall friction factor model. Since no experimental results of the rotordynamic characteristics has been published to date, it is difficult to directly show that the present analysis represents an improvement. Therefore, the theoretical results of Scharrer(1988) using the Blasius' wall friction factor model are compared with the results of the present analysis. The geometries and operating conditions of the teeth-on-rotor stepped labyrinth gas seal, just the same as the Scharrer's case, are given in Table 1. The number of teeth is varied from 5 to 15 for the divergent and the convergent stepped labyrinth seals. The surfaces of the rotor and stator are assumed to be smooth. The comparison of the surface friction factor between the Moody's and the Blasius' model for the smooth surfaces is shown as the function of Reynolds number in Fig. 2. In Fig. 2, 0.0001 is used for e/D of the Moody's model and, n=0.07 and m=-0.25 are used for the empirical coefficients of the Blasius' model. For the operating conditions given in Table 1, the Reynolds number of the flow through the seal is about 6×10^4 where the Moody's friction factor yields almost the same as the Blasius', and the choking occurs at the last seal strip.

Figures 6~9 show the comparisons of results of leakage($\dot{m}$), the direct stiffness(K), the cross-coupled stiffness(k), and the direct damping(C) between the present and Scharrer's analysis for the divergent and the convergent stepped labyrinth seals. The predicted leakage level of the present analysis(solid line) is about 20 % less than that of Scharrer's analysis(dashed line) as shown in Fig. 6. The leakage decreases with increased number of teeth and the divergent seal yields greater leakage than the convergent seal for both the present and Scharrer's analysis.

Figure 7 illustrates the result of the direct stiffness coefficient(K) vs. the number of teeth. The present analysis underpredicts the direct

Table 1 Input data for the analysis of stepped labyrinth seal

Stepped labyrinth seal geometry(Teeth on rotor)	
Inlet radius of seal rotor(Rs)	75.6 (mm)
Tooth height(B)	3.175 (mm)
Tooth pitch(L)	2.175(mm)
Step height(d)	1.0(mm)
Tooth width(t_p)	0.152(mm)
Clearance of seal(C_r)	0.127(mm)
Number of stepped labyrinth teeth(NT)	5, 10, 15
Operating condition	
Entrance pressure	7.0 bar
Exit pressure	1.0 bar
Inlet swirl ratio($V_{in}/(R_s\ \omega)$)	1.0
Rotor speed	20,000(RPM)
Temperature	300(K)
Kinematic viscosity(v)	0.0000023(m^2/s)

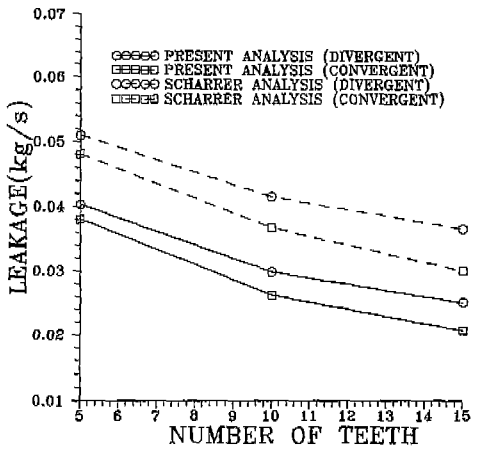

Fig. 6 Leakage prediction for a teeth-on-rotor stepped labyrinth seal

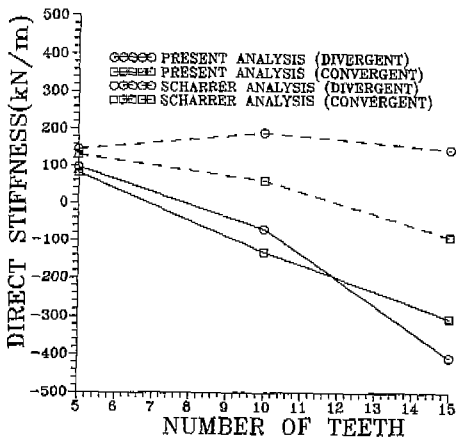

Fig. 7 Direct stiffness coefficient prediction for a teeth-on-rotor stepped labyrinth seal

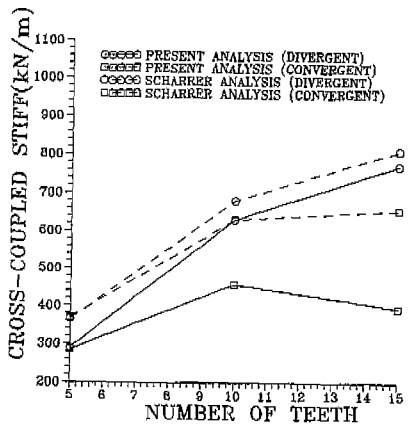

Fig. 8 Cross-coupled stiffness coefficient prediction for a teeth-on-rotor stepped labyrinth seal

stiffness compared with the prediction of Scharrer's analysis. As the number of teeth increases, the difference between the present and Scharrer's analysis increases. Generally, the divergent seal shows greater K than the convergent seal except for the 15-labyrinth teeth seal case of the present analysis.

The cross-coupled stiffness coefficient(k) represents the tangential component of the seal's rotordynamic force acting on the rotor which is precessing in the direction of rotation. The positive cross-coupled stiffness which increases the forward precessing motion has a destabilizing effect. Figure 8 shows that the present analysis predicts smaller cross-coupled stiffness compared with Scharrer's theoretical analysis. For the divergent seal, k rapidly increases as the number of teeth increases. However, the rate of increase of k as the number of teeth increases for the over 10-teeth convergent seals decreases. In particular, the present analysis yields that k decreases as the number of teeth increases for the over 10-teeth convergent seals. Generally, the divergent seal shows greater k than the convergent seal.

The direct damping coefficient(C) represents the tangential component of the seal's rotordynamic force which opposes the preces-

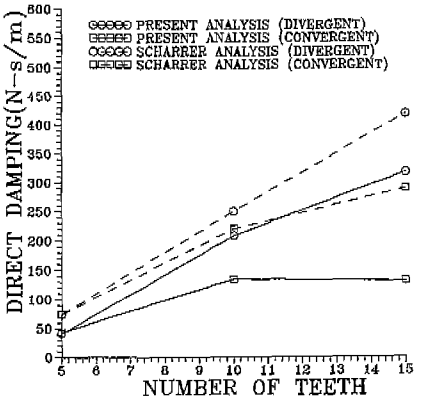

Fig. 9 Direct damping coefficient prediction for a teeth-on-rotor stepped labyrinth seal

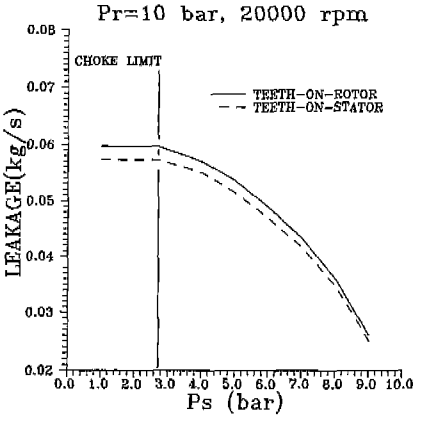

Fig. 10 Leakage vs. exit pressure for a divergent stepped labyrinth seal(NT=5, Inlet swirl ratio=1.0)

sional motion and has a stabilizing effect. The present analysis predicts smaller direct damping coefficient compared with Scharrer's analysis, and the characteristics of C for variations in the number of teeth show a trend similar to those of k.

Figures 10~11 illustrate the simulated leakage and rotordynamic coefficients for the 5-teeth divergent stepped labyrinth seal with the change in exit pressure while the entrance pressure(10 bar) is held constant. The teeth-on-stator seal(dashed line) shows smaller leakage than the teeth-on -rotor seal(solid line), and the choking phenomenon occurs at the exit pressure of 2.7 bar (choke limit). The teeth-on-stator seal shows larger direct stiffness(K) than the teeth-on-rotor

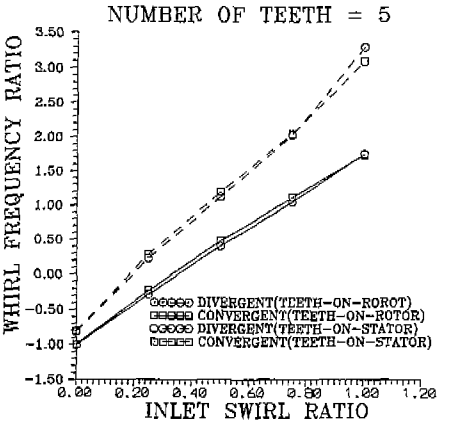

Fig. 11 Rotordynamic coefficients vs. exit pressure for a divergent stepped labyrinth seal(NT= 5, Inlet swirl ratio=1.0)

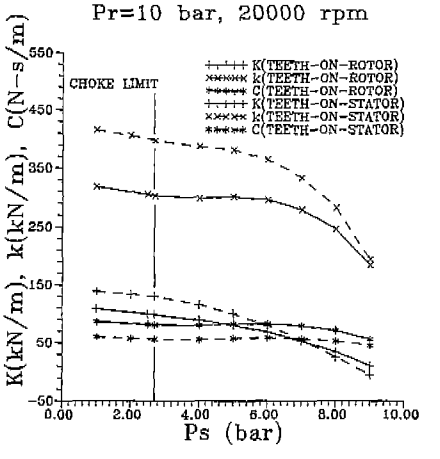

Fig. 12 Whirl frequency ratio vs. inlet swirl ratio for 5-labyrinth teeth seal

seal in the exit pressure range of under 7 bar. For the cross-coupled stiffness(k), the teeth-on-stator seal shows larger value than the teeth-on-rotor seal, but the teeth-on-rotor seal shows larger direct damping(C) than the teeth-on-stator seal. Figure 11 shows that the choking phenomenon does not significantly influence the characteristics of the rotordynamic coefficients.

The whirl frequency ratio($K/\omega C$) is the ratio of the destabilizing forces to the stabilizing forces and should be minimized from the rotordynamic point of view. Figures 12~13 illustrate the comparisons of the whirl frequency ratio versus

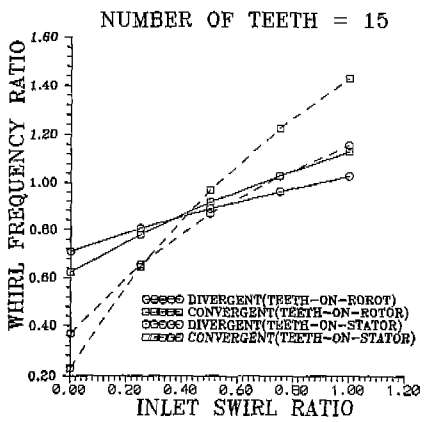

Fig. 13 Fig. 13 Whirl frequency ratio vs. inlet swirl ratio for 15-labyrinth teeth seal

the inlet swirl ratio for the 5-teeth and the 15-teeth stepped labyrinth seal, respectively. The whirl frequency ratio increases as the inlet swirl ratio increases. For the 5-teeth seal, the teeth-on-rotor(solid line) seal is more stable than the teeth-on-stator seal(dashed line) for both the divergent and the convergent stepped labyrinth seal. However, this trend is not true for all inlet swirl ratios in the case of the 15-teeth seal as shown in Fig. 13.

As previously discussed, the rotordynamic characteristics of the stepped labyrinth seal are dependent on the seal geometries and the operating conditions. Therefore, the sophisticated rotordynamic and stability analyses that take into account the detailed seal geometries and operation conditions for the stepped labyrinth seals are required for the vibration analysis of turbomachinery.

5. Conclusions

The leakage prediction and rotordynamic analysis for the stepped labyrinth gas seal are developed by assuming the bulk-flow and using the Moody's wall friction factor model. Although the predictions on the leakage and rotordynamic coefficients can not be directly shown to be more accurate due to a lack of experimental data, the present analysis represents an improvement in that a better friction factor model which is effective for a wider range of the Reynolds number flow and that also takes into account the relative roughness effect is incorporated. The results of the present analysis is compared with the theoretical results of Scharrer's analysis that uses the Blasius' wall friction factor model. The results presented support the following conclusions.

(1) The present analysis shows a good agreement of leakage characteristics with Scharrer's analysis, but underpredicts by about 20 %. The leakage decreases with increased number of stepped labyrinth seal teeth, and the divergent stepped labyrinth seal yields greater leakage than the convergent stepped labyrinth seal.

(2) The present analysis underpredicts the direct stiffness compared to Scharrer's analysis. The divergent stepped labyrinth seal gives greater K than the convergent stepped labyrinth seal except for the 15-labyrinth teeth seal case.

(3) The present analysis shows a similar trend on the cross-coupled stiffness and the direct damping characteristics compared with Scharrer's analysis. However, the present analysis predicts smaller cross-coupled stiffness and direct damping coefficient than Scharrer's analysis. Generally, the divergent stepped labyrinth seal shows greater k and C than the convergent stepped labyrinth seal.

(4) For the 5-teeth seal, the teeth-on-rotor seal is more stable than the teeth-on-stator seal for both the divergent and the convergent stepped labyrinth seal. However, this trend is not true for all inlet swirl ratios for the 15-teeth seal.

References

Alford, J. S., 1965, "Protecting Turbomachinery from Self-Excited Rotor Whirl," *ASME Trans. Journal of Engineering for Power*, pp. 333~344.

Childs, D. W., and Scharrer, J. K., 1986, "An Iwatsubo Based Solution for Labyrinth Seals: A Comparison to Experimental Results," *ASME Trans. Journal of Engineering for Gas Turbines and Power*, Vol. 108, pp. 325~331.

Gurevich, M. I., 1966, *The Theory of Jets In an Ideal Fluid*, Pergamon Press, London, England,

pp. 319~323.

Ha. T. W., and Childs, D. W., 1996, "A Rotordynamic Analysis of an Annular Honeycomb Seal Using a Two-Control Volume Model," *KSME International Journal*, Vol. 10, No. 3, pp. 332~340.

Ha. T. W., and Lee, A. S., 1998, "Rotordynamic Analysis of Compressor Labyrinth Seals," *Journal of KSNVE*, Vol 8, No. 5, pp. 849~855.

Iwatsubo, T., 1980, "Evaluation of Instability Forces of Labyrinth Seals in Turbines or Compressors," NASA CP 2133 Proceedings of a workshop at Texas A&M University 12-14 May Entitled Rotordynamic Instability Problems in High Performance Turbomachinery, pp. 139-167.

John, J. E. A., 1979, Gas Dynamics, Wylic.

Jenny, R. J., Wyssmann, H. P., and Pham, T. C., 1984, "Prediction of Stiffness and Damping Coefficients for Centrifugal Compressor Labyrinth Seals," ASME 84-GT-86. Presented at the 29th International Gas Turbine Conference and Exhibit, Amsterdam, The Netherlands.

Neumann, K. 1964, "Zur Frage der Verwendung von Durchblickdichtungen im Dampgturbinebau," Maschinentechnik, 13(4).

Scharrer, J. 1987, "A Comparison of Experimental and Theoretical Results for Labyrinth Gas Seals," Ph. D. Dissertation, Texas A&M University.

Scharrer, J. K., 1988, "Rotordynamic Coefficients for Stepped Labyrinth Gas Seals," *ASME/ASLE Tribology Conference*, Paper No. 88-Trib-42.

Vermes, G., 1961, "A Fluid Mechanics Approach to the Labyrinth Seal Leakage Problem," *ASME Journal of Engineering for Power*, Vol. 83, No. 2, pp. 161-169.

Appendix

$$G_{1i}=\frac{L_i(Cr_i+B_i)}{Z_cRT};\quad G_{2i}=\frac{(Cr_i+B_i)V_{0i}L_i}{R_{si}RTZ_c};$$

$$G_{3i}=\frac{P_{0i}L_i(Cr_i+B_i)}{R_{si}Z_cRT};$$

$$G_{4i}=\frac{\dot{m}_iP_{0i}}{P_{0i}^2-P_{0i+1}^2}+\frac{\dot{m}_iP_{0i}}{P_{0i-1}^2-P_{0i}^2}+\frac{\dot{m}_i\mu_{1i+1}}{\pi}$$
$$(5-4S_{1i-1})\left(\frac{\gamma-1}{\gamma P_{0i+1}}\right)\left(\frac{P_{0i}}{P_{0i+1}}\right)^{-\frac{1}{\gamma}}$$
$$+\frac{\dot{m}_i\mu_{1i}}{\pi}(5-4S_{1i})\left(\frac{\gamma-1}{\gamma P_{0i}}\right)(S_{1i}+1)$$

$$G_{5i}=-\frac{\dot{m}_i\mu_{1i}}{\pi}(5-4S_{1i})\left(\frac{\gamma-1}{\gamma P_{0i}}\right)\left(\frac{P_{0i-1}}{P_{0i}}\right)^{-\frac{1}{\gamma}}$$
$$-\frac{\dot{m}_iP_{0i-1}}{P_{0i-1}^2-P_{0i}^2}$$

$$G_{6i}=-\frac{\dot{m}_i\mu_{1i+1}}{\pi}(5-4S_{1i+1})\left(\frac{\gamma-1}{\gamma P_{0i+1}}\right)(S_{1i-1}+1)$$
$$-\frac{\dot{m}_iP_{0i+1}}{P_{0i}^2-P_{0i+1}^2};\quad G_{7i}=\dot{m}_i\left(\frac{Cr_i-Cr_{i+1}}{Cr_iCr_{i+1}}\right)$$

$$G_{8i}=\frac{P_{0i}L_i}{Z_cRT};\quad G_{9i}=\frac{P_{0i}V_{0i}L_i}{R_{si}Z_cRT}$$

$$Z_{1i}=\frac{P_{0i}(Cr_i+B_i)L_i}{Z_cRT};\quad Z_{2i}=\frac{(Cr_i+B_i)L_i}{R_{si}Z_cRT}P_{0i}$$

$$V_{0i};\quad Z_{3i}=\frac{L_i(Cr_i+B_i)}{R_{si}};\quad Z_{4i}=\dot{m}_i-\frac{a_{ri}(L_i+d)}{2}\frac{}{Z_cRT}P_{0i}\frac{a_1}{3}$$
$$\left(\frac{a_2e}{Dh_{0i}}+\frac{a_3\nu}{Dh_{0i}(R_{si}\omega-V_{0i})}\right)^{-\frac{2}{3}}\frac{a_3\nu}{Dh_{0i}}$$
$$-\frac{a_{si}(L_i+d)}{2}\frac{}{Z_cRT}P_{0i}\frac{a_1}{3}\left(\frac{a_2e}{Dh_{0i}}+\frac{a_3\nu}{Dh_{0i}V_{0i}}\right)^{-\frac{2}{3}}\frac{a_3\nu}{Dh_{0i}}$$
$$+\frac{2\tau_{r0i}a_{ri}(L_i+d)}{(R_{si}\omega-V_{0i})}+\frac{2\tau_{s0i}a_{si}(L_i+d)}{V_{0i}}$$

$$Z_{5i}=-\dot{m}_i$$

$$Z_{6i}=-\frac{\tau_{r0i}(L_i+d)a_{ri}}{P_{0i}}+\frac{\tau_{s0i}(L_i+d)a_{si}}{P_{0i}}$$
$$-\frac{\dot{m}_iP_{0i}(V_{0i}-V_{0i-1})}{P_{0i-1}^2-P_{0i}^2}$$
$$-\frac{(V_{0i}-V_{0i-1})}{P_{0i}}\frac{\dot{m}_i\mu_{1i}}{\pi}(5-4S_{1i})\left(\frac{\gamma-1}{\gamma}\right)(S_{1i}+1)$$

$$Z_{7i}=\frac{\dot{m}_iP_{0i-1}(V_{0i}-V_{0i-1})}{P_{0i-1}^2-P_{0i}^2}+\frac{(V_{0i}-V_{0i-1})}{P_{0i}}\frac{\dot{m}_i\mu_{1i}}{\pi}$$
$$(5-4S_{1i})\left(\frac{\gamma-1}{\gamma}\right)\left(\frac{P_{0i-1}}{P_{0i}}\right)^{-\frac{1}{\gamma}}$$

$$Z_{8i}=-\frac{(V_{0i}-V_{0i-1})\dot{m}_i}{Cr_i}$$
$$-\frac{a_{ri}(L_i+d)}{2}\frac{}{Z_cRT}P_{0i}(R_{si}\omega-V_{0i})^2\frac{a_1}{3}$$
$$\left(\frac{a_2e}{Dh_{0i}}+\frac{a_3\nu}{Dh_{0i}(R_{si}\omega-V_{0i})}\right)^{-\frac{2}{3}}$$
$$\times\left(\frac{a_2e}{Dh_{0i}^2}+\frac{a_3\nu}{Dh_{0i}^2(R_{si}\omega-V_{0i})}\right)$$
$$\frac{2L_i(L_i+d)}{(Cr_0+B_i+L_i+d)^2}$$
$$+\frac{a_{si}(L_i+d)}{2}\frac{}{Z_cRT}P_{0i}V_{0i}^2\frac{a_1}{3}\left(\frac{a_2e}{Dh_{0i}}+\frac{a_3\nu}{Dh_{0i}V_{0i}}\right)^{-\frac{2}{3}}$$
$$\times\left(\frac{a_2e}{Dh_{0i}^2}+\frac{a_3\nu}{Dh_{0i}^2V_{0i}}\right)-\frac{2L_i(L_i+d)}{(Cr_0+B_i+L_i+d)^2}$$

$a1=1.375\times10^{-3}$, $a2=20000$, $a3=1\times10^6$